Humidity sensors based on ZnO/TiO(2) core/shell nanorod arrays with enhanced sensitivity

Gu, L ; Zheng, K ; Zhou, Y ; Li, J ; Mo, X ; Patzke, Greta R ; Chen, G

Abstract: Highly aligned arrays of ZnO/TiO(2) core/shell nanorods were fabricated on glass substrates by hydrothermal growth of ZnO nanorods cores followed by the deposition of anatase TiO(2) shells in a sol-gel process. The characterization of these composite materials with scanning electron microscopy (SEM), Raman spectroscopy, X-ray diffraction (XRD), energy dispersive X-ray spectroscopy (EDX) and transmission emission microscopy (TEM) points to the formation of crystalline ZnO nanorod cores that are coated with anatase TiO(2) shells. Humidity sensors based on these core/shell nanorod arrays exhibit outstanding sensitivities with capacitances varying from 10(1) to 10(6) pF over a relative humidity (RH) range of 11%-95% at room temperature, which is 1.5 and 3 orders of magnitude higher than that of pristine TiO(2) films and ZnO nanorods, respectively. Complex impedance analysis indicated that the enhanced humidity sensitivity is probably due to the high surface/volume ratio of this core/shell material in combination with the remarkable hydrophilicity of the TiO(2) shell.

DOI: https://doi.org/10.1016/j.snb.2010.12.024

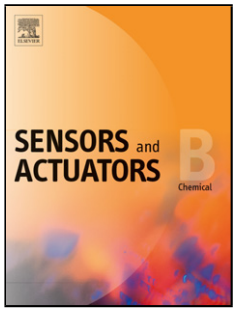

Title: Humidity sensors based on ZnO/TiO_2 core/shell nanorod arrays with enhanced sensitivity

Authors: Leilei Gu, Kaibo Zheng, Ying Zhou, Juan Li, Xiaoliang Mo, Greta R. Patzke, Guorong Chen

PII: S0925-4005(10)00954-8
DOI: doi:10.1016/j.snb.2010.12.024
Reference: SNB 12769

To appear in: *Sensors and Actuators B*

Received date: 31-5-2010
Revised date: 26-10-2010
Accepted date: 15-12-2010

Please cite this article as: L. Gu, K. Zheng, Y. Zhou, J. Li, X. Mo, G.R. Patzke, G. Chen, Humidity sensors based on ZnO/TiO_2 core/shell nanorod arrays with enhanced sensitivity, *Sensors and Actuators B: Chemical* (2010), doi:10.1016/j.snb.2010.12.024

Humidity sensors based on ZnO/TiO_2 core/shell nanorod arrays with enhanced sensitivity

Leilei Gu[a], Kaibo Zheng[a], Ying Zhou[b], Juan Li[a], Xiaoliang Mo[a,*], Greta R. Patzke[b], Guorong Chen[a, *]

[a] Department of Materials Science, Fudan University, Shanghai 200433, PR China
[b] Institute of Inorganic Chemistry, University of Zurich, CH-8057, Switzerland

[*]Corresponding author:

(Guorong Chen)
Tel. +86 (0)21 6564 2873-801
Fax. +86 (0)21 6564 2873
E-mail: grchen@fudan.edu.cn

(Xiaoliang Mo)
Tel. +86 (0)21 6564 2873-801
Fax. +86 (0)21 6564 2873
E-mail:xlmo@fudan.edu.cn

Abstract

Highly aligned arrays of ZnO/TiO_2 core/shell nanorods were fabricated on glass substrates by hydrothermal growth of ZnO nanorods cores followed by the deposition of anatase TiO_2 shells in a sol-gel process. The characterization of these composite materials with scanning electron microscopy (SEM), Raman spectroscopy, X-ray diffraction (XRD), energy dispersive X-ray spectroscopy (EDX) and transmission emission microscopy (TEM) points to the formation of crystalline ZnO nanorod cores that are coated with anatase TiO_2 shells. Humidity sensors based on these core/shell nanorod arrays exhibit outstanding sensitivities with capacitances varying from 10^6 to 10^1 pF over a relative humidity (RH) range of 11% - 95% at room temperature, which is 1.5 and 3 orders of magnitude higher than that of pristine TiO_2 films and ZnO nanorods, respectively. Complex impedance analysis indicated that the enhanced humidity sensitivity is probably due to the high surface/volume ratio of this core/shell material in combination with the remarkable hydrophilicity of the TiO_2 shell.

Keywords: ZnO/TiO_2, core/shell materials, nanorod arrays, capacitance, humidity sensors

1. Introduction

Recently, humidity sensors have attracted considerable research attention due to their key technical applications, such as in process control, meteorology, agriculture, and medical instrumentation [1-3]. Although many oxides, including SnO_2 [4], ZrO_2 [5], SiO_2 [6], have been investigated for humidity sensor development, many novel materials and fabrication methods remain to be explored. Further research is requested to optimize the sensor characteristics, e.g. sensitivity, low hysteresis, excellent stability and short response/recovery times, so that these challenges are in the focus of current science.

As both ZnO and TiO_2 are exceptionally versatile semiconductor materials, they have been widely investigated with respect to their implementation in humidity sensors. Humidity sensors based on one-dimensional (1D) ZnO nanostructures excel through high chemical and physical stability, good sensitivity as well as fast response and recovery time due to their reduced overall dimensions in combination with high surface/volume ratios [7-8]. However, the low hydrophilicity of ZnO materials is an inherent drawback renders their further exploration for humidity sensors with high sensitivities quite difficult. TiO_2 materials are more hydrophilic due to the dissociative adsorption of water at Ti^{3+} defect sites [9] so that their use in humidity sensors has been intensively studied. Nevertheless, the sensing performances of TiO_2 generally suffer from its high resistance, pronounced hysteresis and insufficient long-time stability [10]. In addition, the majority of previous studies was focused on TiO_2 thin films with rather low surface/volume ratios that limit the sensitivity in comparison with 1D nanostructures [11-12]. To solve this problem, porous thin films of TiO_2 have been furthermore investigated as another approach. However, the enhanced sensitivity of porous films was achieved at the cost of manifold problems, e.g. insufficient response and recovery times, poor reproducibility and hysteresis effects [13]. Therefore, the combination of ZnO and TiO_2 as complementary materials is a promising approach to enhance the humidity sensitivity with respect to the binary oxides. Moreover, the fabrication of core/shell heterostructures could lead to additional benefits from the "synergistic" interaction of chemical and physical properties in ZnO/TiO_2 composites. This principle has been frequently reported for core/shell-based gas sensors that displayed enhanced response to ethanol [14], carbon monooxide [15] and sulfurated hydrogen [16], whereas only few investigations on humidity sensors based on core/shell nanomaterials have been published to date.

In this study, ZnO/TiO_2 core/shell nanorod arrays (ZTNA)[1] were fabricated through sol-gel processes to combine the advantages of both components into a single composite material. The obtained core/shell nanocomposites were fabricated as humidity sensor prototypes, and their sensing performance was characterized. Furthermore, sensing mechanisms were derived from analysis of the complex impedance plots.

2. Experimental Section

2.1 Preparative procedures

2.1.1 Synthesis of ZnO seed layers

1.0975 g (5 mmol) of $Zn(Ac)_2 \cdot 2H_2O$ and 0.3 ml of monoethanolamine were dissolved in 100 ml 2-methoxyethanol and sonicated for 20 minutes to obtain a stable and homogeneous solution. The solution was then spin-coated onto a glass substrate followed by exposure to infrared radiation for 2 min to remove the solvent. The whole process was repeated five times. The as-prepared substrates were sintered at 350^{o}C for 30 minutes to yield dense and transparent ZnO seed layers.

2.1.2 Growth of well aligned ZnO nanorod arrays

ZnO nanorod arrays were hydrothermally grown in 150 ml of an aqueous solution of 20 mM zinc acetate ($Zn(Ac)_2 \cdot 2H_2O$) and hexamethylenetetramine (HMTA; $C_6H_{12}N_4$). The solution was then transferred into a sealed vessel where the substrates were suspended in the solution, with the side covered with the seed layer facing the bottom of the vessel. The vessel was covered with a piece of glass, heated and kept at 93^{o}C for 6 h whilst the solution was refreshed every 2 h. Afterwards, the substrates were recovered, rinsed several times with deionized water and dried at 60^{o}C for 10 minutes.

2.1.3 Coating of ZnO nanorods with TiO_2 shells

The coating with TiO_2 shells was achieved through sol-gel methods. The sol was prepared as follows: 8.7 ml of tetrabutylorthotitante and 2.8 ml of diethanolamine were dissolved in 35 ml of ethanol. After magnetic stirring for 2 h, 0.45 ml of deionized water mixed with 4.5 ml of ethanol were added dropwise into the above solution under stirring. After another 2 hours of stirring, the sol was aged under light exclusion for 24 h.

The procedure for the growth of TiO_2 shells is analogous to the protocol used for the ZnO seed

[1] ZTNA: ZnO/TiO_2 core/shell nanorod array

layers except that substrates covered with ZnO nanorod arrays have to be immersed in the sol for 1 min before spin-coating. Afterwards, as-obtained substrates were transferred into a tube furnace, sintered in air at 550^{o}C for 1 h and then cooled down to room temperature naturally, thereby leading to the formation of ZTNAs.

2.1.4 Assembly of humidity sensors

ZTNA sensors were fabricated by in-situ growth of ZnO/TiO_2 nanocomposites on glass surfaces coated with previously deposited Au/Ni interdigitated electrodes. Sensors based on ZnO nanorods and on TiO_2 thin films were assembled in the same way as humidity sensing reference materials. Au/Ni interdigitated electrodes, with an effective area of 0.8×0.5 cm^2 were deposited by thermal evaporation utilizing a shadow mask.. Bars and gaps of the individual electrodes were equidistant (200 μm).

2.2 Characterization

2.2.1 Materials characterization

All samples were morphologically characterized by scanning electron microscopy (SEM) performed on a Zeiss SUPRA 50VP microscope with a voltage of 2 kV without further coating. All products were structurally characterized through X-ray diffraction (XRD) recorded on a Rigaku powder X-ray diffractometer using Cu K_α radiation (40 kV, 100 mA). The compositions of the composite materials were studied by energy dispersive X-ray spectroscopy (EDX) and the microstructures of the composite materials were investigated by transmission electron microscopy (TEM, TECANI F20). Raman spectroscopy was recorded on a confocal microscope (Dilor, France, LABRAM-1B) using the polarized line at 632.8 nm of a He: Ne laser at room temperature. Brunauer-Emmett-Teller (BET) surface area measurements were performed on an Autosorb 1 in N_2-adsorption mode. Complex impedance measurements (Nyquist diagrams) were performed on a PAR 2273 electrochemical station (frequency range: 20 Hz - 1 MHz).

2.2.2 Humidity sensor characterization

The electrical characteristics of the sensors were tested as a function of relative humidity (RH) with a TH2617 LCR analyzer (Changzhou, China) with an applied AC voltage of 1 V and 1 kHz in a home-built testing chamber. The chamber was filled with saturated solutions of LiCl, $MgCl_2$, $Mg(NO_3)_2$, KCl and KNO_3, respectively, to calibrate the RH to 11%, 33%, 55%, 75%, 85% and

95% at room temperature. The sensors were suspended in the above sealed chamber without contacting the solution and they were stored in a dry environment after the test runs. A schematic illustration of the sensing tests is provided in Fig. 1. The sensor was equaled to a capacitance (C_p) in parallel with a resistance (R_p). The former (C_p) was the one recorded at different humidities.

3. Results and discussion

3.1 Structure and morphology of ZTNA

Phase purity and crystal structure of the as-obtained sensor materials were evaluated with XRD analyses. Fig. 2a displays the XRD pattern of the pristine samples prior to the coating process. All diffraction peaks can be indexed to the hexagonal wurtzite structure of ZnO (JCPDS No. 36-1451; S.G. $P6_3mc$, a = 3.24982(9) Å, c = 5.2066(15) Å). The sharp and predominant peak observed at $2\theta=34.4^o$ (002) indicates the high degree of crystallinity of the ZnO nanorods and points to their perpendicular growth on the substrate along [0001], i.e. along the *c* axis. However, after the coating process, additional peaks were observed (Fig. 2b) indicating the presence of other phases (represented by circles). The peak at 37.6^o can be assigned to the (004) plane of anatase TiO_2, whereas the weaker peaks of $Zn_{1.7}SiO_4$ and Zn_2TiO_4 indicate a reaction between the sample and the glass substrate and the interaction of ZnO core and TiO_2 shell, respectively. The simultaneous presence of both ZnO and anatase TiO_2 diffraction peaks after coating demonstrates the co-existence of both phases.

Fig. 3a displays a typical SEM image of as-obtained ZnO seed layers, exhibiting uniform ZnO particles with a diameter of ca. 200 nm. SEM images of the hydrothermally grown ZnO nanorods and ZnO/TiO_2 core/shell nanomaterials are shown in Fig. 3b and c, respectively. ZnO nanorods are grown perpendicular to the substrate with an average diameter of 200 nm, as expected from the size of the ZnO seeds (cf. Fig. 3a). The nanorod shape can be maintained after coating with the TiO_2 shells, but the surface of the composite materials became rougher and the mean diameter increased to ca. 220 nm: this indicates the deposition of a TiO_2 layer on the ZnO rods. The BET surface areas of ZnO nanorods and ZTNA (16.4 and 16.7 mm^2/g, respectively) demonstrate the high surface/volume ratio of the core/shell material. EDX recorded at the upper ends of the ZnO/TiO_2 nanorods further confirm the presence of titanium, oxygen and zinc in the nanorods. High-resolution TEM investigations of the composite materials are shown in Fig. 3d. The

observed fringes correspond to two different interplanar distances of 0.26 nm and 0.24 nm which agree well with the lattice spacings of the (002) ZnO plane and of the (103) anatase TiO_2 plane. These results furthermore indicate the deposition of anatase TiO_2 nanoparticles on the surface of ZnO nanorods.

The Raman spectra of the ZnO nanorod arrays before (a) and after coating (b) are compared in Fig. 4. All peaks observed for pristine ZnO could be assigned to the reference data for ZnO. The intense peak at 438 cm^{-1} can be identified as the E_2 (high) mode, corresponding to the characteristic band of the hexagonal wurtzite ZnO phase. The peaks located at 334 cm^{-1} and 381 cm^{-1} correspond to the $3E_{2H}$-E_{2L} and A_1 (TO) modes, respectively [17]. After coating with TiO_2, the E_g mode of anatase TiO_2 [18] was observed as an additional peak at 142 cm^{-1} (cf. symbols in Fig. 4), thereby providing additional evidence for the deposition of the anatase modification which agrees well with the results from XRD and HRTEM investigations. Moreover, no peaks were apparently observed at the A_1 (LO) mode position of 576 cm^{-1} before and after coating: this indicates that the ZnO nanorod arrays maintain their high degree of crystallinity during the thermal treatment with minimal additional defects (such as O-vacancies, Zn-interstitials, or complexes thereof) [19]. Therefore, the resulting variation of chemical and physical properties is dominated by the TiO_2 modification rather than by the variation of defects in the ZnO nanorods. In addition, as shown by the dashed lines, no significant shift was observed for the E_2 mode position of ZNTA at 438 cm^{-1}, thereby pointing to a minimum extent of both compressive and tensile stress [20]. The interactions between ZnO core and TiO_2 shell are thus minimal so that most of the TiO_2 nanoparticles are attached to the surface of ZnO nanorods rather than being firmly intergrown with the crystal lattice.

3.2 Humidity sensing performance

In order to study the synergistic effect of the combination of the ZnO nanorods with a TiO_2 layer on the resulting humidity sensing performance, sensors based on pristine ZnO nanorods,TiO_2 thin films and ZTNAs were fabricated (cf. section 2.1.4.) and their humidity sensing properties were compared.

Fig. 5a shows the capacitance response curves of the sensors based on TiO_2 film, ZnO nanorod arrays and ZTNA for selected RH values ranging from 11% to 95%. All sensor types display reproducible sensing responses. The response of the ZnO sample is proportional to the water

vapor concentration over the entire investigated RH range. However, this linear behavior applies only up to 85% RH for TiO_2 films and ZTNA sensors. The RH dependent sensitivity values, defined as the ratio of the capacitance measured for the actual vapor concentration to the respective value for 11% RH, are compared in Fig. 5b. The sensitivity of the sensors based on ZTNAs is considerably enhanced in comparison with the sensors fabricated from the individual components. The sensitivity of the ZTNA sensors at 95% RH is about 8.96E4, thus being 31 and 1380 times higher than that of pristine ZnO nanorod arrays (2.9E3) and TiO_2 film (65) based sensors, respectively. Furthermore, it should be mentioned that the ZTNA sensors show a superior sensitivity not only with respect to pure ZnO and TiO_2 but also in comparison with modified ZnO and TiO_2 nanofibers (e.g. with LiCl and KCl as dopants) [21-23]. The notably enhanced sensitivity probably results from the larger surface area of ZnO nanorods that renders them an ideal substrate for surface coating with hydrophilic TiO_2 particles.

Moreover, response and recovery behavior are the key characteristics to evaluate the performance of humidity sensors as shown in Fig. 6. The actual values of response and recovery time upon exposure to 95% RH (defined as the time to achieve 90% of the total capacitance change in the case of adsorption and desorption process, respectively) are summarized for all three sensor types in Table 1. All of them exhibit fast response and recovery processes and the recovery time spans exceed the response periods. The sensor based on TiO_2 film showed the fastest response and recovery to water vapor due to its low surface/volume ratio, whereas the ZnO nanorod arrays–based sensor exhibited the longest response and recovery times. The ZTNA sensors display intermediate values with respect to the ZnO and TiO_2-based sensors, indicating that the temporal response of these humidity sensors could be optimized by fine-tuning the composition of the sensing layer. In addition, not only the sensitivity of ZTNA sensors is much higher than that of other two sensors, but their response and recovery times are also shorter than those of the sensor constructed from ZnO nanorod arrays. These results demonstrated that the enhanced sensitivity of ZTNA did not come at the cost of delayed response and recovery times compared to the ZnO nanorod arrays sensor.

Fig. 7a shows the reproducibility of the response curves of ZTNA sensors under ambient conditions for the RH range from 11% to 95%. The stable maximum and minimum capacitance values confirm the good reproducibility of ZTNA sensors. The results furthermore demonstrate

that the interaction between water vapor and the surface of the nanorods is dominated by physisorption. Otherwise a baseline drift resulting from the incomplete desorption during chemisorption could be observed, because the bonding energy between the adsorbed molecules and the surface of nanorods of chemisorptions is much higher than that of physisorption [24].

The humidity hysteresis characteristics of the ZTNA based humidity sensor are shown in Fig. 7b. The black line (squares) represents the adsorption process, and the red line (circles) stands for the desorption process. Both lines are close with maximum deviation at 33% RH: this points to a threshold value for the transition between two different sensing mechanisms that are discussed in the following part (cf. 3.3).

3.3 Sensing mechanism

The sensing mechanisms of the above-mentioned humidity sensors were investigated through the analysis of complex impedance plots. The complex impedance plots (Nyquist diagrams) of sensors based on pristine ZnO nanorod arrays and on ZTNAs in the range of 20 Hz ~1 MHz are displayed in Fig. 8a-b. A semicircular Nyquist diagram indicates that the ZTNA sensor could be represented by parallel circuits of a resistor (R_a) and a capacitor (C_a), as shown in Fig. 9 a, where R_a and C_a are the resistance and capacitance of the nanorod arrays, respectively. R_a is corresponding to the real impedance at low frequency limiting and C_a can be achieved from the imaginary part. This semicircular Nyquist diagram indicates that the ZTNA sensor operates through a hopping mechanism, i.e. the discrete jump of charge carriers from one site to another over energy barriers. Under this circumstance, no continuous aquatic layer is formed owing to the insufficient adsorption of water vapor [25-27].

With increasing adsorption, a linear tail occurred at lower frequencies accompanied by a significant decrease of the semicircular part. A basic element, Warburg impedance, was added in series with R_a to the equivalent circuit (Fig 9 b), which represents the involvement of diffusion of reactants [28]. If the adsorption is increased further, the resulting Nyquist diagram is a 45^o line for all frequencies. Here, the electrolytic conduction mainly arises from the faster diffusion of protons in single or multilayers that are formed on the materials surface [29-30]. This facilitates carrier transportation and favors polarization as well, thereby allowing for a large capacitance response.

The transition threshold of the two sensing mechanisms for the ZTNA based sensors is about 33% RH at room temperature in contrast to the transition point of 75% RH for the uncoated sample

(Fig. 8). In contrast to the absence of straight line plots for the sensors based on pristine ZnO nanorods at high frequencies even at 95% RH, a straight line at full frequency range was observed at 55% RH for the ZTNA based sensors. In combination with the decreasing value for the transition threshold, this behavior indicates that TiO_2 coating enhances water adsorption on the sensor surface. The adsorption process is domineered by the rough surface of the TiO_2 shell and its remarkable hydrophilicity. With the increment of humidity values, a capillary condensation takes place in the pores with smaller radius than the Kelvin critical radius on the surface of TiO_2 and the ZnO/TiO_2 interface [31], as shown in Fig 10. The formation of these pores is due to the nanoscale grain boundaries of the TiO_2 shell [32].

All in all, the introduction of the TiO_2 shell leads to the adsorption of more water molecules by increasing the hydrophilicity of the surface area and by inducing capillary condensation. This furthermore favors the polarization of the adsorbed water molecules and gives rise to accelerated capacitance response.

4. Conclusions

Vertically aligned ZnO nanorod arrays were grown hydrothermally and subsequently coated with a TiO_2 layer in a sol-gel process. The formation of a crystalline ZnO/TiO_2 composite was confirmed through SEM, XRD, HRTEM and Raman spectroscopy investigations. The analytical results in their entirety demonstrated that the majority of the anatase TiO_2 nanoparticles are located at the surface of ZnO nanorods instead of being doped into the ZnO lattice. The comparison of the humidity sensing performances of pristine TiO_2 films, ZnO nanorods and ZTNA showed that the humidity sensing properties were considerably enhanced through coating of the nanorod template with an anatase TiO_2 shell. The response and recovery behavior of the substrate was not affected by the composite formation. The analysis of complex impedance plots of both ZnO nanorods and ZTNA sensors in terms of equivalent circuit models was applied to assign detailed sensing mechanisms to these sensor types. The results underscore that the surface morphology and the high degree of hydrophilicity lead to the enhanced adsorption facilities and humidity sensing properties of the ZnO/TiO_2 nanorod arrays. This demonstrates how the sensing properties of binary oxides can be combined in a “synergistic” fashion through the synthesis of nanostructured composites.

Acknowledgements:

This work has been funded by the Science and Technology Commission of Shanghai Municipality (NO: 09DZ1142102)

References:

[1] Z. M. Rittersma, Recent achievements in miniaturized humidity sensors - a review of transduction techniques, Sens. Actuators A 96 (2002) 196-210.

[2] C. Y. Lee, G. B. Lee, Humidity sensors: a review, Sens. Lett. 3 (2005) 1-15.

[3] K. M. Willett, N. P. Gillett, P. D. Jones, P. W. Thorne, Attribution of observed surface humidity changes to human influence, Nature 446 (2007) 710-712.

[4] W. P. Tai, J. H. Oh, Fabrication and humidity sensing properties of nanostructured TiO_2-SnO_2 thin films, Sens. Actuators B 85 (2002) 154-157.

[5] M. K. Jain, M. C. Bhatnagar, G. L. Sharma, Effect of Li^+ doping on ZrO_2–TiO_2 humidity sensor, Sens. Actuators B 55 (1999) 180-185.

[6] P. Innocenzi, A. Martucci, M. Guglielmi, A. Bearzotti, E. Traversa, Electrical and structural characterisation of mesoporous silica thin films as humidity sensors, Sens. Actuators B 76 (2001) 299-303.

[7] Q. Wan, Q. H. Li, Y. J. Chen, T. H. Wang, X. L. He, X. G. Gao, J. P. Li, Positive temperature coefficient resistance and humidity sensing properties of Cd-doped ZnO nanowires, Appl. Phys. Lett. 84 (2004) 3085-3087.

[8] Q. Qi, T. Zhang, Q. J. Yu, R. Wang, Y. Zeng, L. Liu, H. B. Yang, Properties of humidity sensing ZnO nanorods-base sensor fabricated by screen-printing, Sens. Actuators B 133 (2008) 638-643.

[9] G. Montesperelli, A. Pumo, E. Traversa, G. Gusmano, A. Bearzotti, A. Montenero, G. Gnappi, Sol-gel processed TiO_2-based thin films as innovative humidity sensors, Sens. Actuators B 25 (1995) 705-709.

[10] H. K. Kim, S. D. Sathaye, Y. K. Hwang, S. H. Jhung, J. S. Hwang, S. H. Kwon, S. E. Park, J. S. Chang, Humidity sensing properties of nanoporous TiO_2-SnO_2 ceramic sensors, Bull. Korean Chem. Soc. 26 (2005) 1881-1884.

[11] A. Bearzotti, A. Bianco, G. Montesperelli, E. Traversa, Humidity sensitivity of sputtered TiO_2 thin films, Sens. Actuators B 9 (1994) 525-528.

[12] G. Gusmano, G. Montesperelli, P. Nunziante, E. Traversa, A. Montenero, M. Braghini, G. Mattogno, A. Bearzotti, Humidity-sensitive properties of titania films prepared using the sol-gel process, J. Ceram. Soc. Jp. 101 (1993) 1095-1100.

[13] K. Katayama, K. Hasegawa, T. Takahashi, T. Akiba, H. Yanagida, Humidity sensitivity of Nb_2O_5-doped TiO_2 ceramics, Sens. Actuators A 24 (1990) 55-60.

[14] Y. J. Chen, C. Zhu, T. H. Wang, The enhanced ethanol sensing properties of multi-walled carbon nanotubes/SnO_2 core/shell nanostructures, Nanotechnology 17 (2006) 3012-3017.

[15] M. M. Maye, Y. B. Lou, C. J. Zhong, Core−shell gold nanoparticle sssembly as novel electrocatalyst of CO oxidation, Langmuir 16 (2000) 7520-7523.

[16] X. Y. Xue, L. L. Xing, Y. J. Chen, S. L. Shi, Y. G. Wang, T. H. Wang, Synthesis and H_2S sensing properties of CuO-SnO_2 core/shell PN-junction nanorods, J. Phys. Chem. C 112 (2008) 12157-12160.

[17] T. C. Damen, S. P. S. Porto, B. Tell, Raman effect in zinc oxide, Phys. Rev. 142 (1966) 570-574.

[18] W. F. Zhang, Y. L. He, M. S. Zhang, Z. Yin, Q. Chen, Raman scattering study on anatase TiO_2 nanocrystals, J. Phys. D: Appl. Phys. 33 (2000) 912-916.

[19] F. J. Manjon, B. Mari, J. Serrano, A. H. Romero, Silent raman modes in zinc oxide and related nitrides, J. Appl. Phys. 97 (2005) 053516.

[20] M. Kubal, Raman spectroscopy of GaN, AlGaN and AlN for process and growth monitoring/control, Surf. Interface Anal. 31 (2001) 987-999.

[21] Q. Qi, T. Zhang, L. J. Wang, Improved and excellent humidity sensitivities based on KCl-doped TiO_2 electrospun nanofibers, Appl. Phys. Lett. 93 (2008) 023105.

[22] Z. Y. Li, H. N. Zhang, W. Zheng, W. Wang, H. M. Huang, C. Wang, A. G. MacDiarmid, Y. Wei, Highly sensitive and stable humidity nanosensors based on LiCl doped TiO_2 electrospun nanofibers, J. Am. Chem. Soc. 130 (2008) 5036-5037.

[23] W. Wang, Z. Li, L. Liu, H. N. Zhang, W. Zheng, Y. Wang, H. M. Huang, Z. J. Wang, C. Wang, Humidity sensor based on LiCl-doped ZnO electrospun nanofibers, Sens. Actuators B 141 (2009) 404-409.

[24] J. A. Robinson, E. S. Snow, F.K. Perkins, Improved chemical detection using single-walled carbon nanotube network capacitors, Sens. Actuators A 135 (2007) 309-314.

[25] K. Ogura, T. Tonosaki, H. Shiigi, AC Impedance spectroscopy of humidity sensor using poly(o)/(vinyl alcohol) composite film, J. Electrochem. Soc. 148 (2001) H21-H27.

[26] Y. Li, M. J. Yang, Y. She, Humidity sensors using in situ synthesized sodium polystyrenesulfonate/ZnO nanocomposites, Talanta 62 (2004) 707-712.

[27] E. Traversa, A. Bearzotti, M. Miyayama, H. Yanagida, Study of the conduction mechanism of La_2CuO_4-ZnO heterocontacts at different relative humidities, Sens. Actuators B 25 (1995) 714-718.

[28] M. Vrnata, D. Kopeckı, F. Vyslouzil, V. Myslik, P. Fitl, O. Ekrt, J. Hofmann, L. Kucera, Impedance properties of polypyrrolic sensors prepared by MAPLE technology, Sens. Actuators B 137 (2009) 88-93.

[29] C. D. Feng, S. L. Sun, H. Wang, C. U. Stetter, Humidity sensing properties of nafion and sol-gel derived SiO_2/nafion composite thin films, Sens. Actuators B 40 (1997) 217-222.

[30] J. Wang, Q. H. Lin, R. Zhou, B. K. Xu, Humidity sensors based on composite material of nano-$BaTiO_3$ and polymer RMX, Sens. Actuators B 81 (2002) 248-253.

[31] J. T. W. Yeow, J. P. M. She, Carbon nanotube-enhanced capillary condensation for a capacitive humidity sensor, Nanotechnology 17 (2006) 5441-5448.

[32] P. Chauhan, S. Annapoorni, S.K. Trikha, Humidity-sensing properties of nanocrystalline haematite thin films prepared by sol–gel processing, Thin Solid Films 346 (1999) 266–268.

Biographies

Leilei Gu received his B.Sc. degree in Materials Science from Fudan University, Shanghai, China in 2007. He is currently a Master student under the supervision of Prof. G. R. Chen at Fudan University, Shanghai, China. His research interests are in the area of nanowire based sensors.

Kaibo Zheng received his B.Sc. and doctor degree in Materials Science from Fudan University, Shanghai, China in 2005 and 2010. He is currently doing his postdoctoral research under the guidance of Prof. Tonu Pullerits, Chemical Physics Department, Lund University, Lund, Sweden. His research interests are in the areas of electric and optic device application of 1D semiconductor nanostructures.

Ying Zhou received his B.Sc. and M.Sc. degree in Materials Science from Central South University in 2004 and Shanghai Institute of Optics and Fine Mechanics, Chinese Academy of Science in 2007. He received his doctor degree in Prof. G. R. Patzke's group at the University of Zurich, Switzerland in 2010 and currently he is going on his postdoctoral research in the same place. His research interests are in the areas of hydrothermal synthesis, in situ studies and environmental applications of oxide nanomaterials.

Juan Li received his B.Sc. degree in Materials Science from Fudan University, Shanghai, China in 2007. She is currently a Master student under the supervision of Prof. G. R. Chen at Fudan University, Shanghai, China. Her research interests are in the area of solar cells and nanowire based sensors.

Xiaoliang Mo received his B.Sc., M.Sc. and PhD degree in Materials Science from Fudan University, Shanghai, China in 2002. From 2003 to 2007, he worked as researcher of National Institute of Advanced Industrial Science and Technology (AIST) in Japan. Since 2008, he is associate professor at Fudan University, Shanghai, China. His research interests include functional polymer thin films and thin film solar cells.

Greta. R. Patzke was born 1974 in Bremen, Germany, and studied chemistry at the University of Hannover where she received her PhD in 1999. This was followed by Habilitation at ETH Zurich (2006) in the laboratory of Prof. Dr. R. Nesper. Since 2007, she is Assistant Professor (SNSF, Tenure Track) at the Insitute of Inorganic Chemistry, University of Zurich. Her research interests are focused on the development of new oxide-based materials, ranging from nanomaterials over polyoxometalates to hybrid compounds.

Guorong Chen received his B.Sc. degree in Physics from Fudan University, Shanghai, China in 1969. From 1995 to 1997, he worked as researcher and visitor of National Institute of Advanced Industrial Science and Technology (AIST) and Keio University in Japan. He is currently professor in the Department of Materials Science, Fudan University, Shanghai, China. His research interests include nanoelectronics, nano-scaled electric device and nanostructured solar cells.

Figure Captions:

Fig. 1 Schematic representation of the sensor test setup and of the constructed humidity sensors.

Fig. 2 XRD patterns of (a) uncoated and (b) coated samples.

Fig. 3 Representative SEM images of (a) ZnO seed layer; (b) ZnO nanorods; (c) ZTNA and (d) HRTEM image of the ZnO/TiO_2 composite materials

Fig. 4 Raman spectra of (a) pristine ZnO nanorod arrays and (b) ZTNAs.

Fig. 5 (a) Time-dependent capacitance of sensors based on TiO_2 thin film (black) and pristine ZnO nanorod arrays (green) compared to ZTNA sensors (blue) at various humidities; (b) comparison of the concentration-dependent sensitivity of the different sensor types.

Fig.6 Response and recovery times of sensors based on pristine ZnO nanorod arrays, ZTNA and TiO_2 thin film for RH values between 11% and 95%.

Fig.7 (a) reproducibility and (b) hysteresis characteristics of humidity sensors based on ZTNA.

Fig.8 Complex impedance plots of (a) pristine and (b) TiO_2-coated ZnO nanorods for different relative humidities at room temperature.

Fig.9 The equivalent circuits of sensors displaying (a) a hopping mechanism and (b) an ion diffusion mechanism (R_a: resistance of nanorod arrays, C_a: capacitance of nanorod arrays, Z_i: Warburg impedance).

Fig.10 Adsorption models for different nanorod types: (a) pristine ZnO nanorods; (b) ZnO/TiO_2 core/shell nanorods.

Table 1. Response and recovery times of sensors based on TiO_2 films, ZnO nanorods and ZnO/TiO_2 nanorod arrays for the humidity range between 11% RH and 95% RH.

Table 1:

Sample	Response time (s)	Recovery time (s)
ZnO nanorods	990.6	35.4
TiO_2 thin film	178.1	5.9
ZTNAs	774.9	19.7

Figure(s)
Click here to download high resolution image

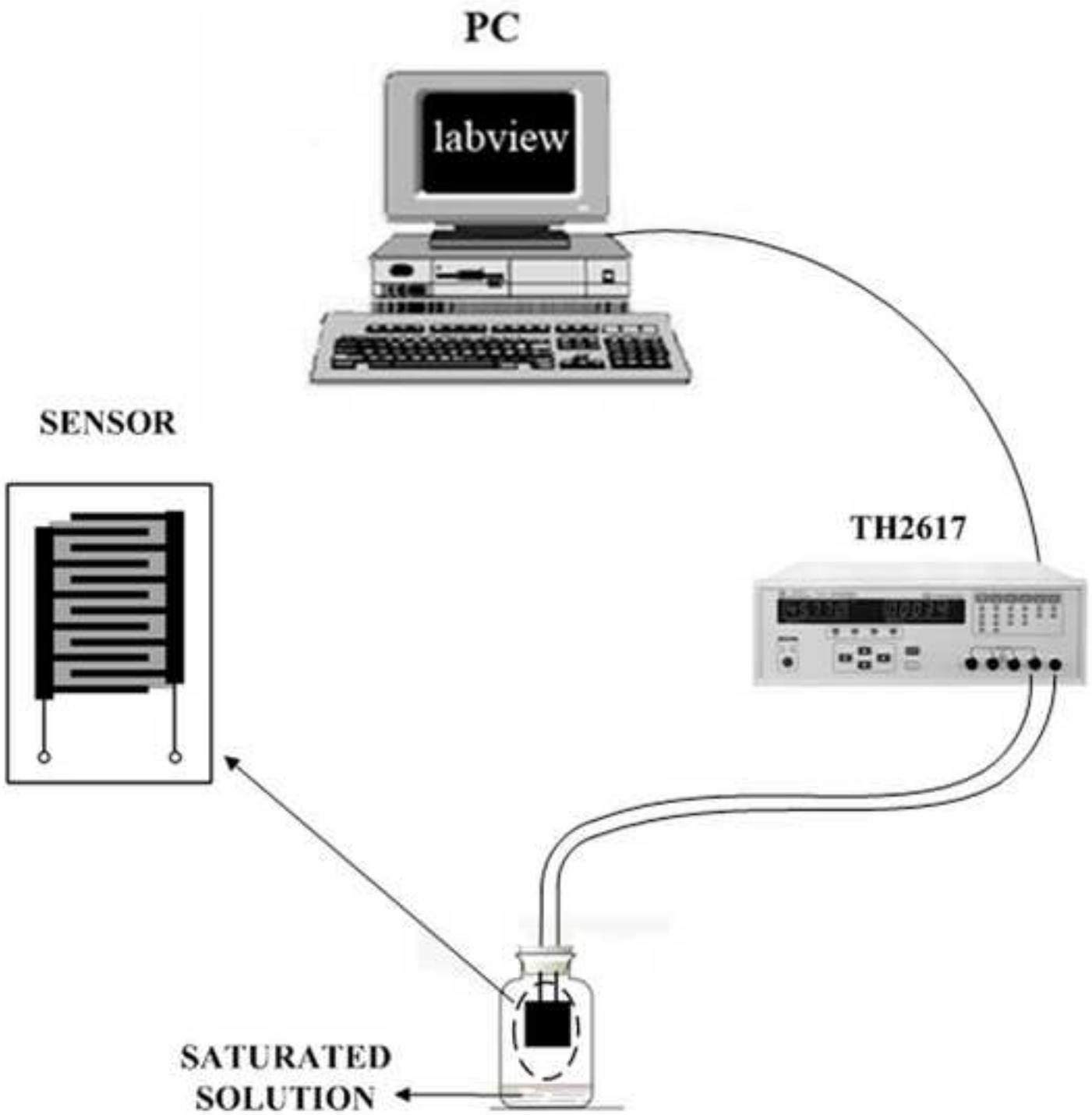

Figure(s)
Click here to download high resolution image

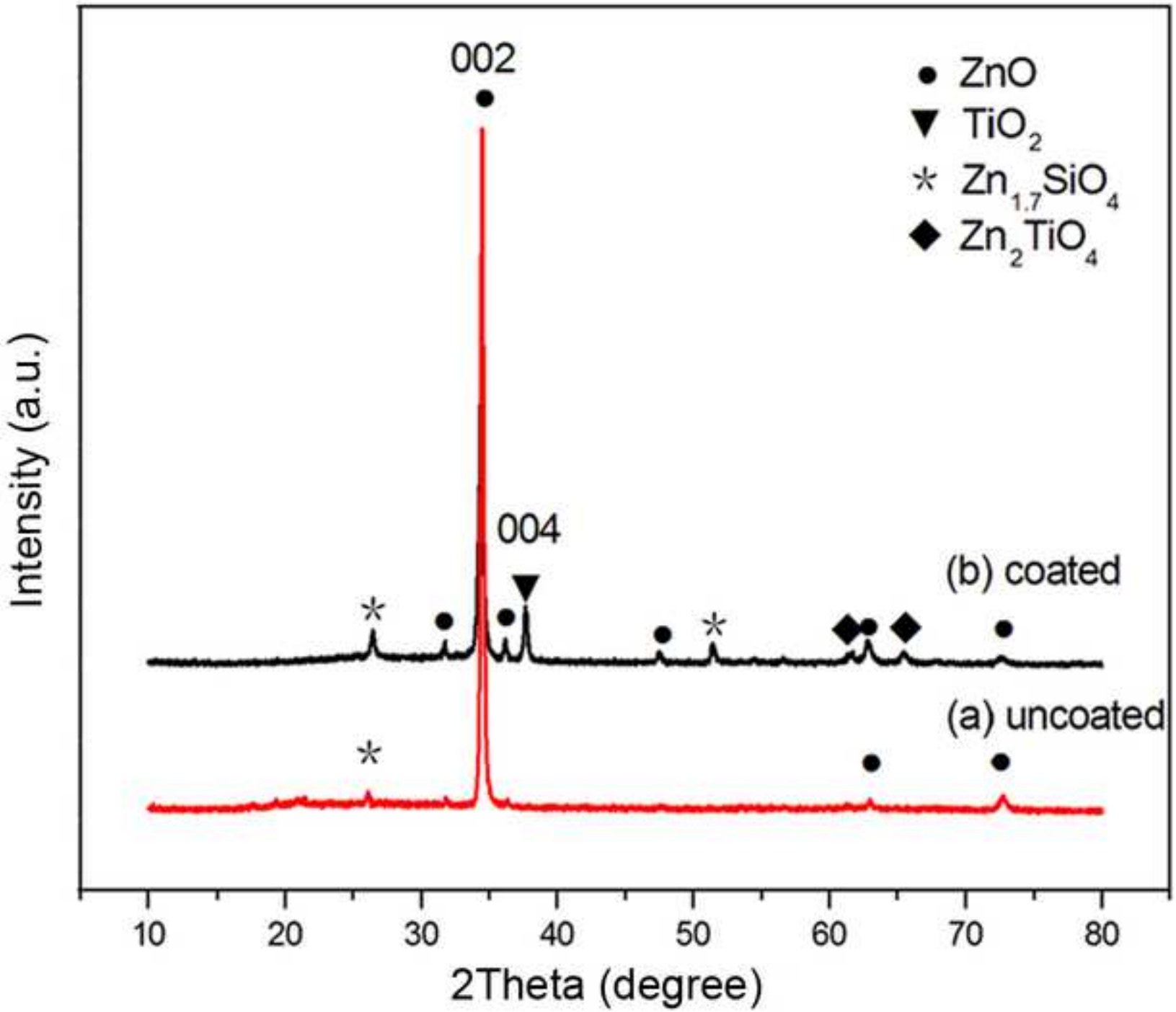

Figure(s)
Click here to download high resolution image

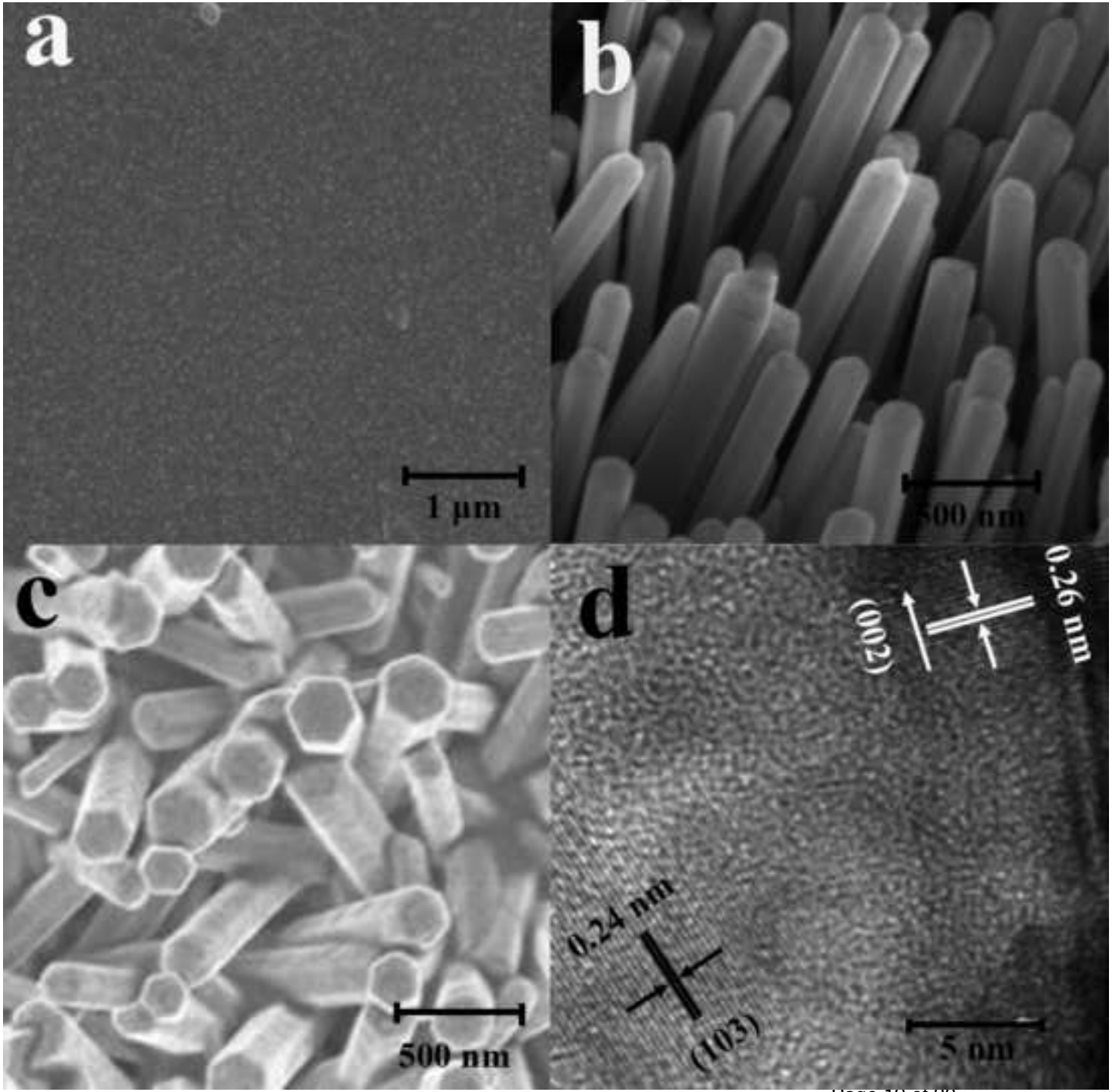

Figure(s)
Click here to download high resolution image

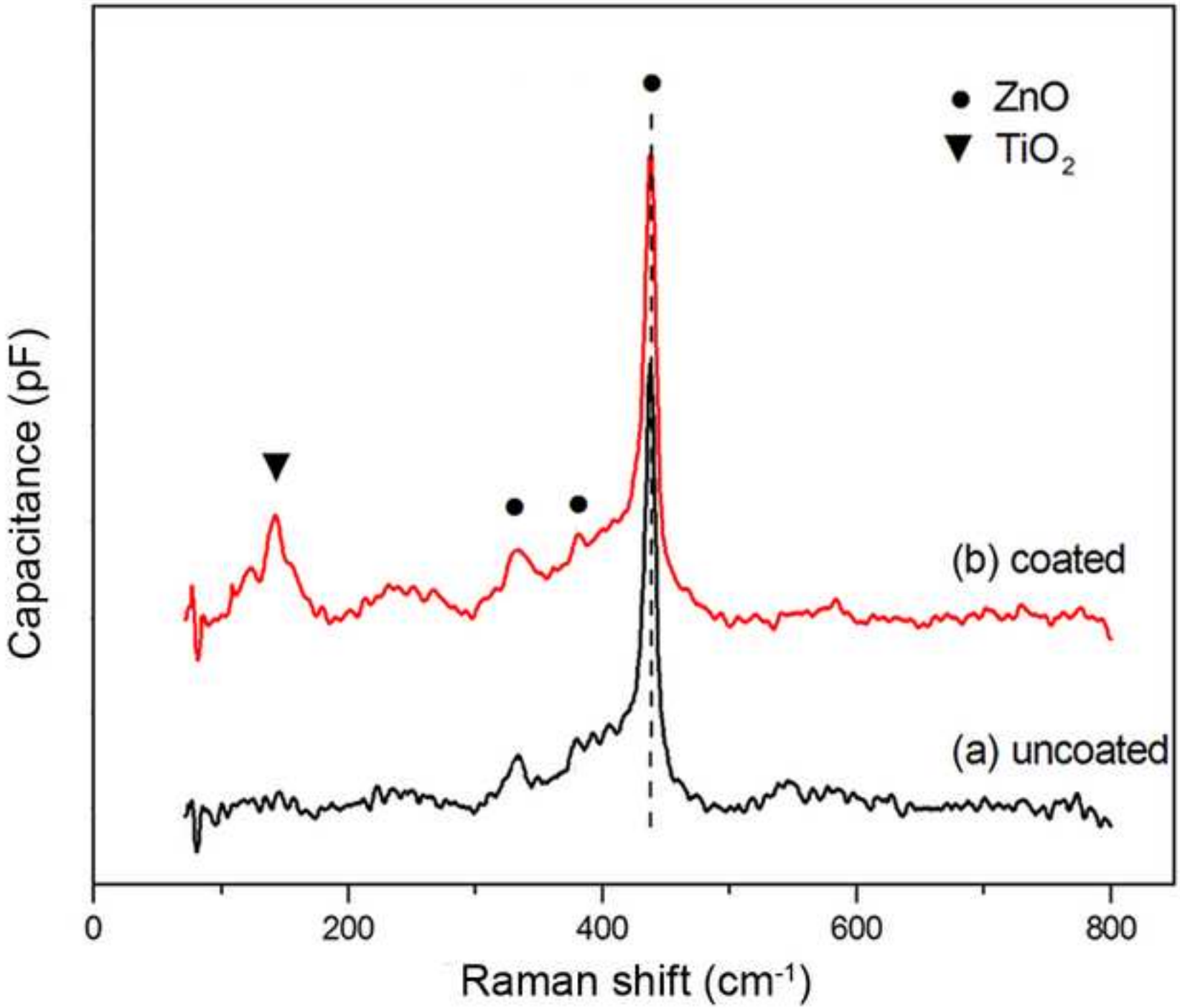

Figure(s)
Click here to download high resolution image

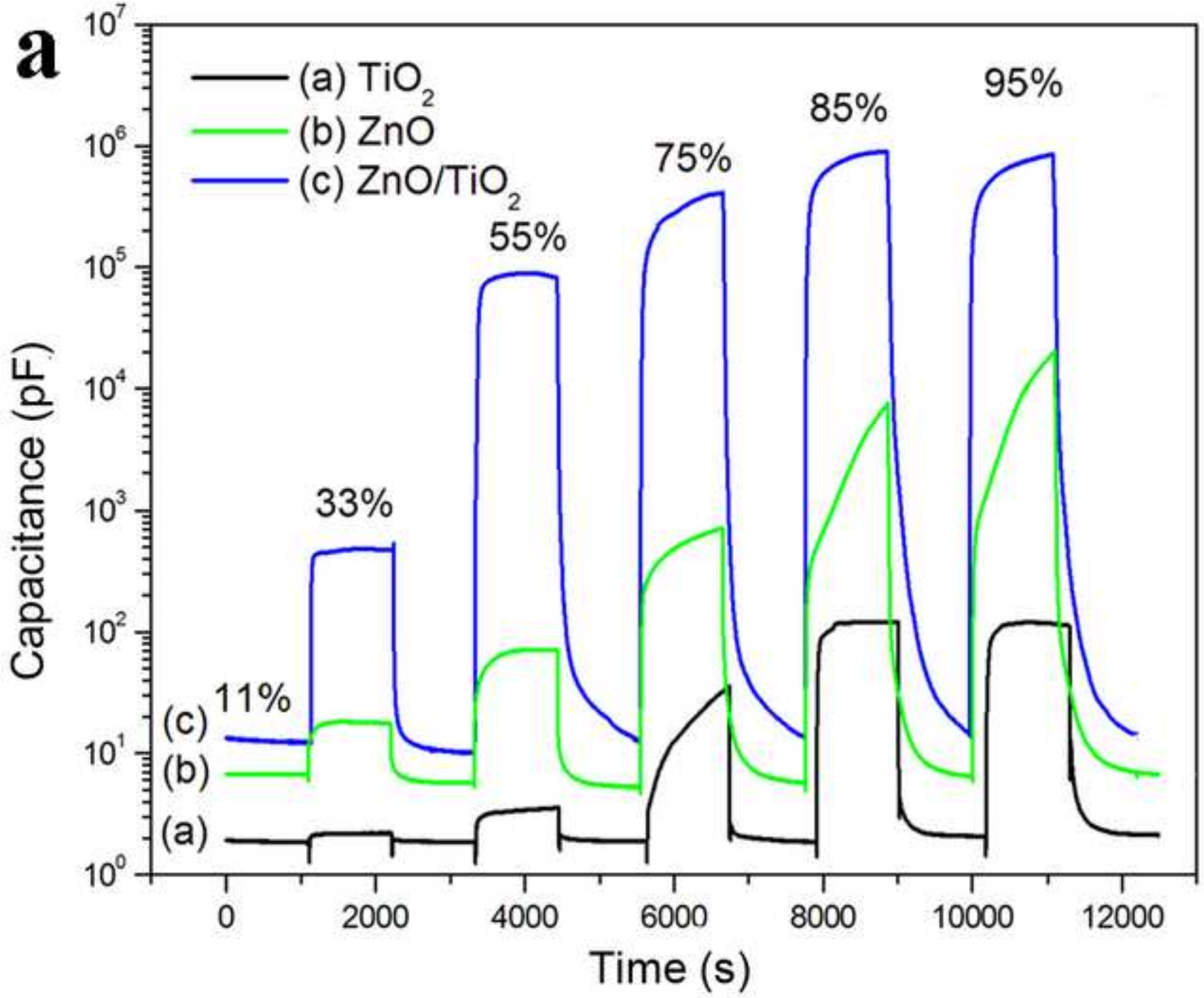

Figure(s)
Click here to download high resolution image

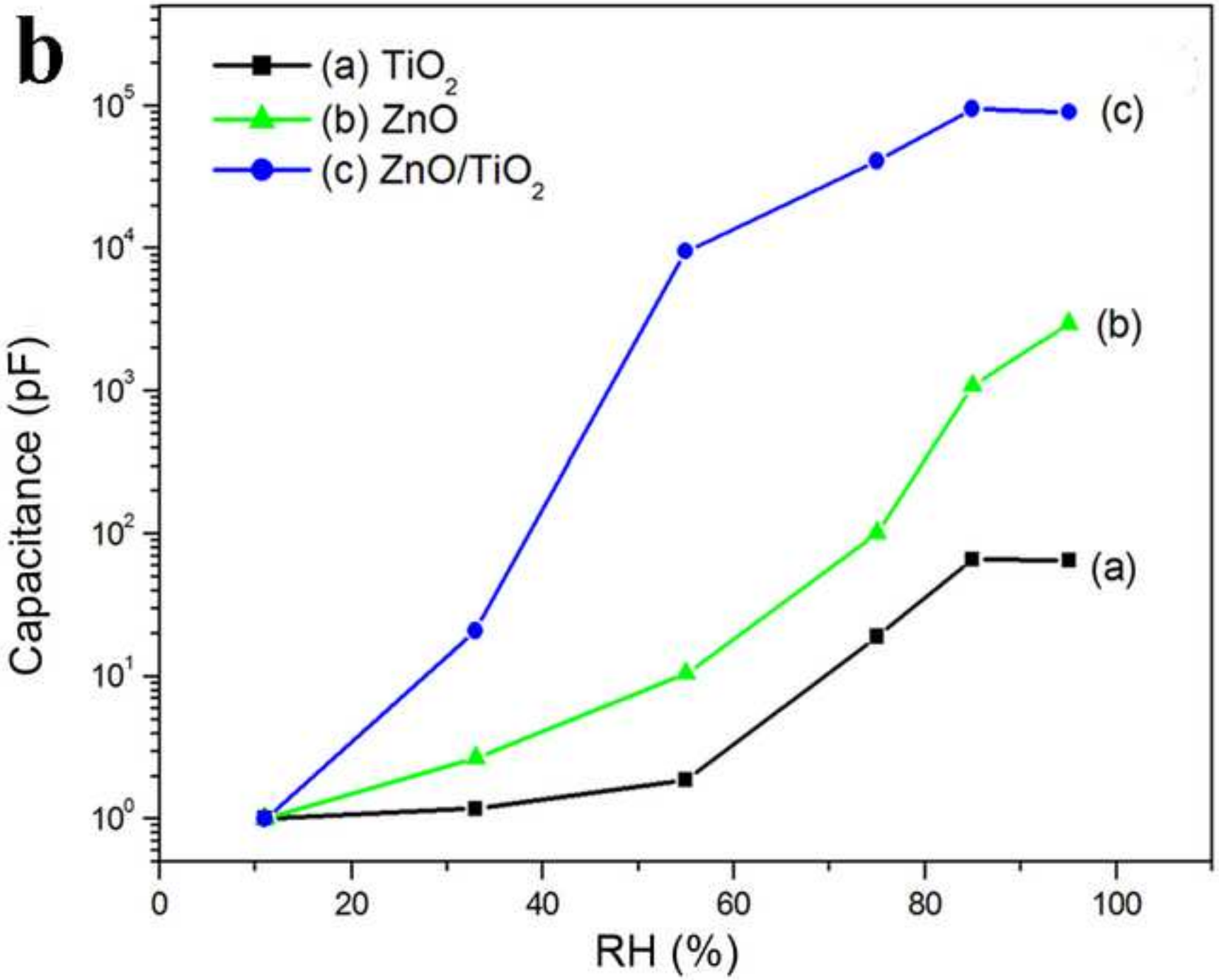

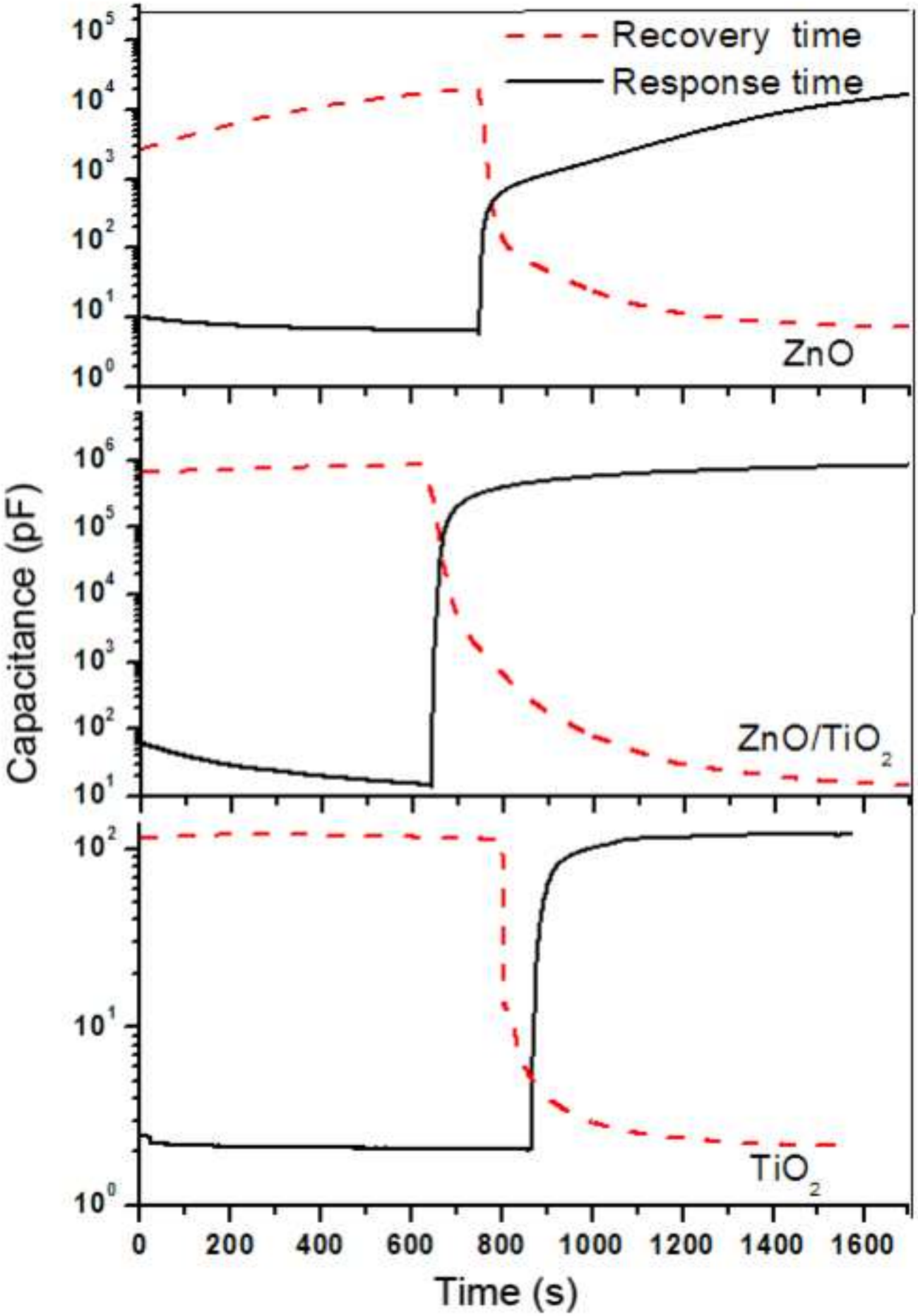

Figure(s)
Click here to download high resolution image

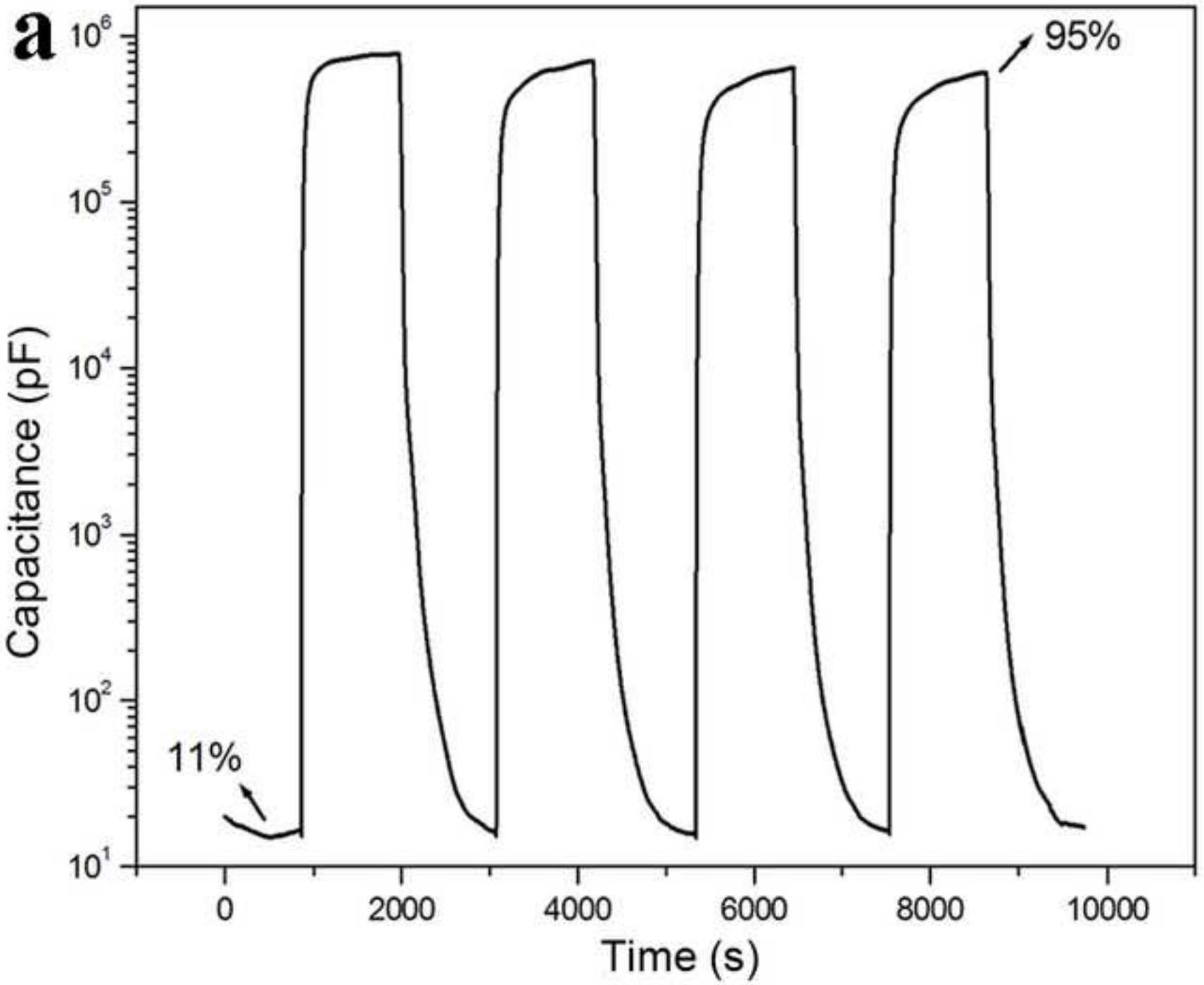

Figure(s)
Click here to download high resolution image

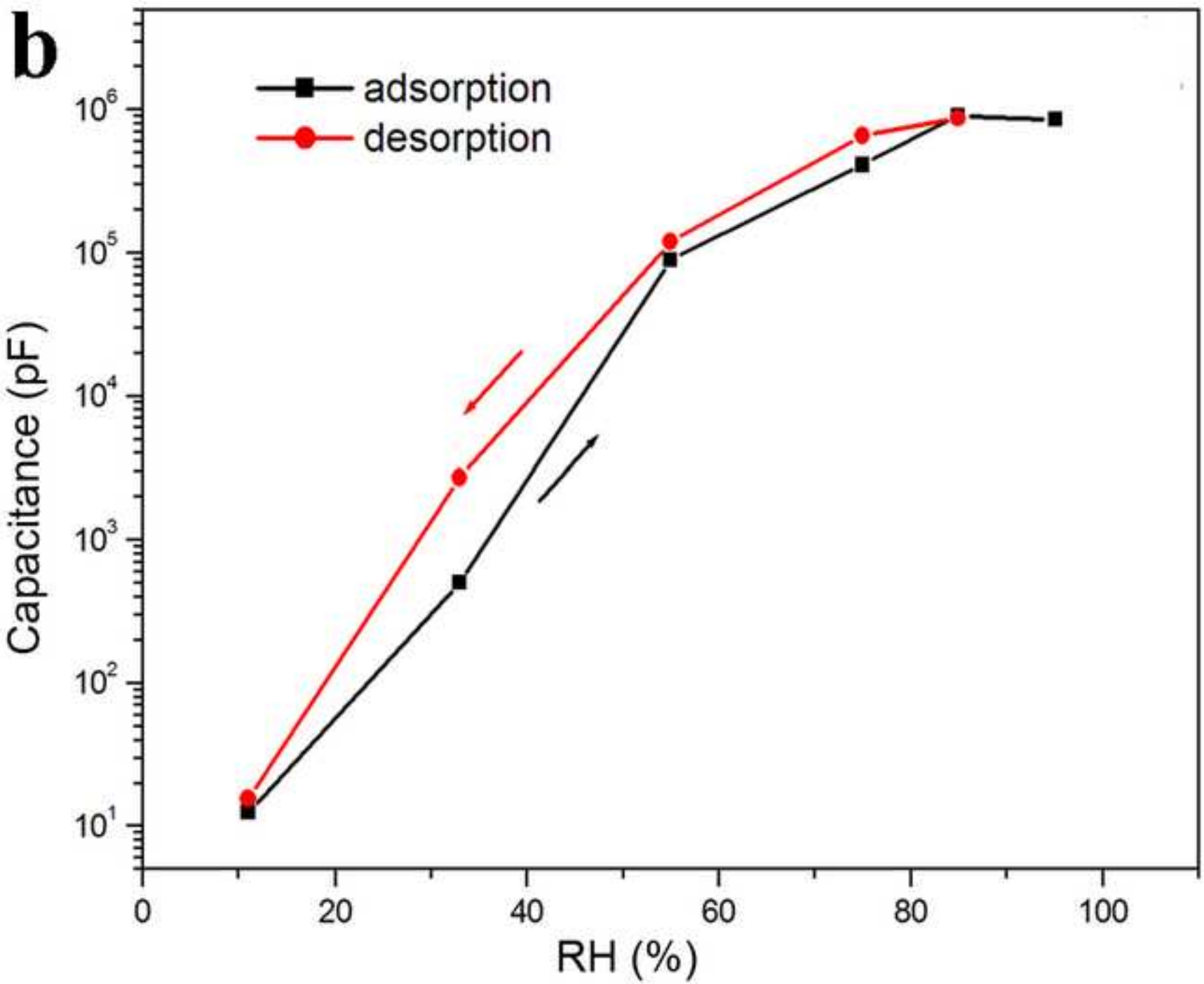

Figure(s)
Click here to download high resolution image

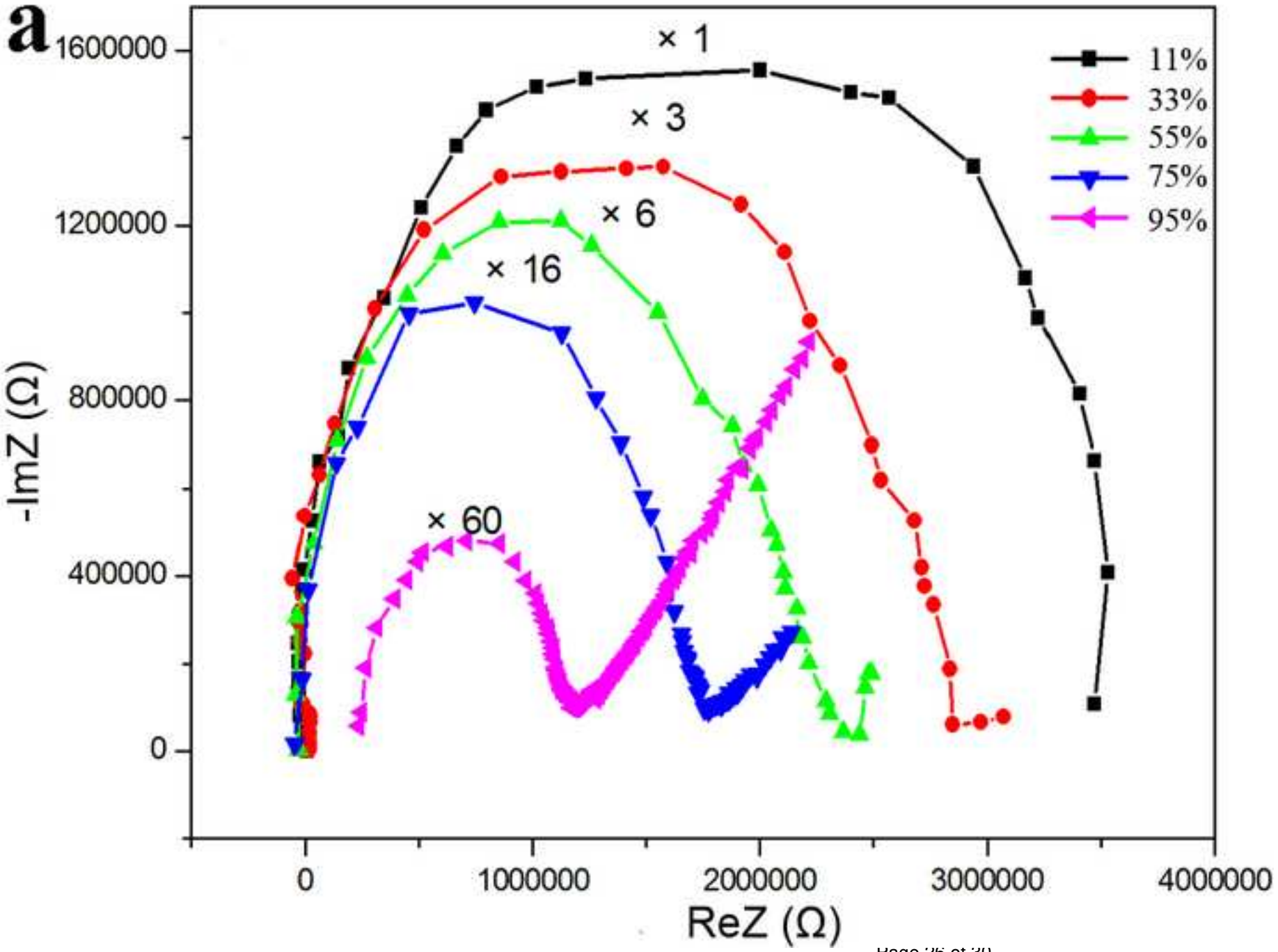

Figure(s)
Click here to download high resolution image

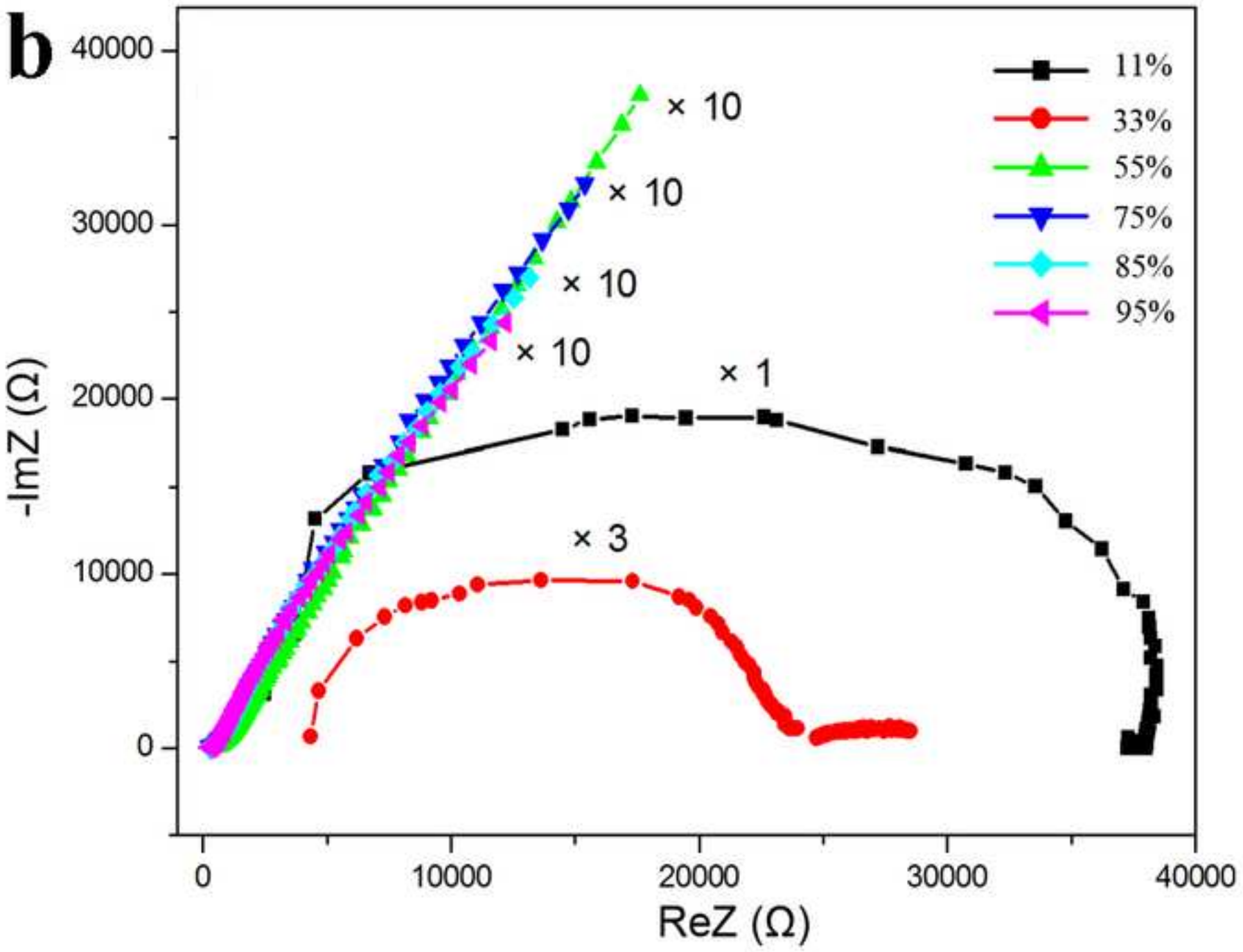

Figure(s)
Click here to download high resolution image